Inorganic Chemistry

Article

pubs.acs.org/IC

Synthesis, Structure, Spectroscopic Characterization, and Protein Binding Affinity of New Water-Soluble Hetero- and Homometallic Tetranuclear $[Cu^{II}_2Zn^{II}_2]$ and $[Cu^{II}_4]$ Clusters

Ayan Patra,[†] Tamal K. Sen,[‡] Atanu Ghorai,[§] Ghezai T. Musie,*[,⊥] Swadhin K. Mandal,[‡] Utpal Ghosh,[§] and Manindranath Bera*[,†]

[†]Department of Chemistry, University of Kalyani, Kalyani, West Bengal 741235, India

[‡]Department of Chemical Sciences, Indian Institute of Science Education & Research Kolkata, Mohanpur, West Bengal 741252, India

[§]Department of Biochemistry and Biophysics, University of Kalyani, Kalyani, Nadia, West Bengal 741235, India

[⊥]Department of Chemistry, The University of Texas at San Antonio, San Antonio, Texas 78249, United States

Supporting Information

ABSTRACT: Two new water-soluble hetero- and homometallic tetranuclear clusters, $Na_4[Cu_2Zn_2(ccdp)_2(\mu\text{-}OH)_2]\cdot CH_3OH\cdot 6H_2O$ (**1**) and $K_3[Cu_4(ccdp)_2(\mu\text{-}OH)(\mu\text{-}OH_2)]\cdot 14H_2O$ (**2**), have been synthesized in methanol–water at room temperature by exploiting the flexibility, chelating ability, and bridging potential of a carboxylate-rich dinucleating ligand, *N*,*N*′-bis(2-carboxybenzomethyl)-*N*,*N*′-bis(carboxymethyl)-1,3 diaminopropan-2-ol (H_5ccdp). Complex **1** is obtained through the self-assembly of two monoanionic $[CuZn(ccdp)]^-$ fragments, which are, in turn, exclusively bridged by two μ-OH^- groups. Similarly, complex **2** is formed through the self-assembly of two monoanionic $[Cu_2(ccdp)]^-$ species exclusively bridged by one μ-OH^- and one μ-OH_2 groups. Complexes **1** and **2** are fully characterized in the solid state as well as in solution using various analytical techniques including a single-crystal X-ray diffraction study. The X-ray crystal structure of **1** reveals that two Cu^{II} centers are in a distorted square-pyramidal geometry, whereas two Zn^{II} centers are in a distorted trigonal-bipyramidal geometry. The solid-state structure of **2** contains two dinuclear $[Cu_2(ccdp)]^-$ units having one Cu^{II} center in a distorted square-pyramidal geometry and another Cu^{II} center in a distorted trigonal-bipyramidal geometry within each dinuclear unit. In the powder state, the high-field EPR spectrum of complex **1** indicates that two Cu^{II} ions are not spin-coupled, whereas that of complex **2** exhibits at least one noninteracting Cu^{II} center coordinated to a nitrogen atom of the ligand. Both complexes are investigated for their binding affinity with the protein bovine serum albumin (BSA) in an aqueous medium at pH ∼7.2 using fluorescence spectroscopy. Synchronous fluorescence spectra clearly reveal that complexes **1** and **2** bind to the active sites in the protein, indicating that the effect is more pronounced toward tyrosine than tryptophan. Density functional theory calculations have been carried to find the Fukui functions at the metal sites in complexes **1** and **2** to predict the possible metal centers involved in the binding process with BSA protein.

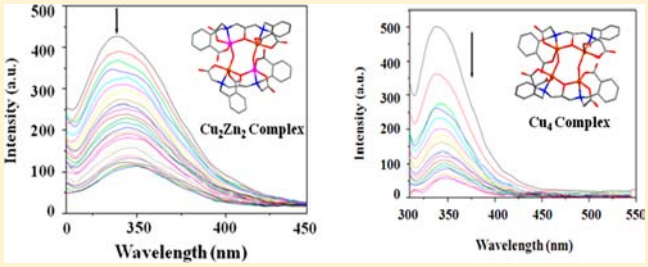

INTRODUCTION

Properly designed hetero- and homometallic multinuclear complex systems not only present synthetic challenges but also can provide novel reactivity patterns as well as physical properties. The neighboring metal centers in multimetallic systems are expected to cooperate in promoting reactions, and new electronic interactions might lead to distinct physical properties. Cooperative interactions have commonly been observed in biological systems, and nature has constructed numerous multimetallic protein complexes that perform an extraordinary array of catalytic transformations.[1−4] This biochemistry has encouraged inorganic chemists to develop the area from an inorganic viewpoint. Furthermore, from the materials viewpoint, the multimetallic complexes can exhibit a full spectrum of new magnetic, optical, and redox properties as a result of a synergetic effect between the different metals.[5−8] Cooperative interactions have been applied in the fields of supramolecular chemistry, enzyme-like catalytic systems, and functional molecular sensors.[9] Furthermore, heterodimetallic complexes offer an enormous potential in the fields of homogeneous catalytic processes.[10] Recently, progress has been documented in the application of M−O−M1-based heterometallic complexes in homogeneous catalytic processes with the concept of dual catalysis.[11] Similarly, the field of molecular-based magnetic materials has shown spectacular advances over the last 2 decades.[12] The advances have rekindled interest in the fields of synthesis and characterization of hetero- and homometallic dinuclear complexes. As a result, a number of hetero- and homometallic dinuclear complexes of copper and zinc are well documented in the literature using both symmetrical and unsymmetrical dinucleating ligands.[13−18] However,

Received: September 27, 2012
Published: March 1, 2013

   dx.doi.org/10.1021/ic302099y | *Inorg. Chem.* 2013, 52, 2880−2890

very little is known about structurally characterized heterometallic tetranuclear $[Cu^{II}_2Zn^{II}_2]$ complexes.[19] Finding such multinuclear hetero- and homometallic complex systems in good yield is indeed a synthetic challenge given the increased complexity of these compounds. Hence, the synthesis and investigation of hetero- and homometallic polynuclear complexes for any purpose warrant filling the void.

Serum proteins play an essential role in the transport and metabolism of Cu^{II} and Zn^{II} ions.[20,21] Moreover, selective quantification of protein is of fundamental importance in basic biochemical or biomedical research and disease treatment. Currently, the available classical methods for protein detection include enzyme-linked immunosorbent assay, Western blotting, and two-dimensional gel electrophoresis, etc.[22] Most of these techniques need rather complicated and laborious assay procedures and expensive materials. Recently, many reports on metal complex−protein interactions have appeared in the literature. However, the majority of the documented works are based on the interactions of mononuclear metal complexes with proteins.[23] Few studies, however, have demonstrated that some multinuclear copper(II) complexes can efficiently promote the binding and cleavage of biological macromolecules such as DNA.[24] The three global pharmacological factors controlling the activity of metal-based drugs are cellular uptake, the frequency and structure of biomolecule adducts, and the extent of metabolizing interactions. The presence of multimetals in the coordination sphere in multinuclear complexes allows modulation of such pharmacological factors and, in turn, may alter the drug efficacy. Moreover, during interaction of a protein substrate with the multinuclear complexes, the influence of the neighboring metal ions cannot be ignored. Binding at one metal center can be favored under the strong electrostatic influence of the other metal ions in the multinuclear complexes. This is in contrast to the mononuclear complexes. In this context, there is a demanding need for multinuclear hetero- and homometallic complexes with proportional variations in the metal ions because of their potential applications in medicinal chemistry such as the development of new metal-based drugs for the binding of different biological macromolecules.[25]

The focus here is on a carboxylate-rich dinucleating ligand, *N*,*N*′-bis(2-carboxybenzomethyl)-*N*,*N*′-bis(carboxymethyl)-1,3 diaminopropan-2-ol (H_5ccdp), with two acetate and two benzoate functionalities (Figure 1). The carboxylate-rich dinucleating ligands

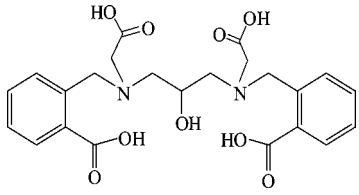

Figure 1. Chemical structure of the ligand H_5ccdp.

have been used for some time as a way to assemble metal ions into aggregates with relevance in the area of bioinorganic chemistry.[26,27] The ligand H_5ccdp is recently known to bind Zn^{II} and Co^{II} ions to yield mono- and hexanuclear zinc(II) complexes and tetranuclear cobalt(II) complexes, showing the bridging potential of carboxylates.[28,29] Very recently, we have reported the synthesis, characterization, and spectroscopic investigations correlating the diverse binding modes of carboxylates of the ligand H_5ccdp in a tetranuclear zinc(II) complex.[30] Recently, the unusual amide and carboxylate binding modes of a similar amide- and carboxylate-rich dinucleating ligand have been explored in a self-assembled heptanuclear zinc complex.[27] In this paper, we report the synthesis, structure, spectral characterization, and bovine serum albumin (BSA) protein binding affinity of new hetero- and homometallic tetranuclear $Cu^{II}_2Zn^{II}_2$ and Cu^{II}_4 clusters.

EXPERIMENTAL SECTION

Materials and Methods. 2-Carboxybenzaldehyde, 1,3-diamino-2-propanol, and iodoacetic acid were purchased from Sigma-Aldrich Chemie GmbH, Germany. Zinc perchlorate hexahydrate and copper perchlorate hexahydrate were prepared in our laboratory following the usual process. Bovine serum albumin (BSA) was purchased from Sigma Chemicals, USA. Calf thymus DNA (CT-DNA) was purchased from SRL, India. All other chemicals and solvents were reagent-grade materials and were used as received from commercial sources without further purification. Microanalyses (C, H, and N) were performed using a Perkin-Elmer 2400 CHNS/O series II elemental analyzer. Fourier transform infrared (FTIR) spectra were obtained on a Perkin-Elmer L120-000A spectrometer (200−4000 cm^{-1}). ^1H and ^{13}C NMR spectra were obtained in a D_2O solution on a Bruker AC 400 NMR spectrometer using tetramethylsilane as the internal standard. Mass spectrometry (MS) spectra were recorded in MALDI-TOF MS using a Perseptive Bio System Voyager DE-STR mass spectrometer. UV−vis spectra were recorded on a Shimadzu UV 1800 (190−1100 nm; 1 cm quartz cell) spectrophotometer. The solution electrical conductivity was obtained with a Systronics 304 digital conductivity meter with a solute concentration of about 10^{-3} M. The room temperature magnetic susceptibilities in the solid state were measured using a home-built Gouy balance fitted with a polytronic direct-current power supply. The experimental magnetic susceptibilities were corrected for the diamagnetic response using Pascal's constants.[31] High-frequency electron paramagnetic resonance (EPR) spectra were recorded on a home-built spectrophotometer at the EMR facility of NHMFL.[32] The instrument was a transmission-type device in which microwaves are propagated in cylindrical light pipes. The microwaves were generated by a phase-locked Virginia Diodes source generating a frequency of 13 ± 1 GHz and producing its harmonics, of which the 4th, 8th, 16th, 24th, and 32nd were available. A superconducting magnet (Oxford Instruments) capable of reaching a field of 17 T was employed.

Synthesis of *N*,*N*′-Bis(2-carboxybenzomethyl)-*N*,*N*′-bis-(carboxymethyl)-1,3-diaminopropan-2-ol (H_5ccdp). The ligand has been prepared according to the previously reported procedure.[28] The product was collected by filtration, washed with water and methanol, and dried at 80 °C. The product was confirmed by elemental analysis, FTIR, and ^1H and ^{13}C NMR spectroscopy. Anal. Calcd for $C_{23}H_{26}N_2O_9\cdot 2HCl$: C, 50.47; H, 5.16; N, 5.12. Found: C, 50.35; H, 5.47; N, 5.01. FTIR (cm^{-1}): ν 3505(b), 3032(b), 1665(s), 1590(vs), 1562(s), 1440(s), 1392(s), 1264(s), 1160(s), 902(s), 846(s), 788(s). ^1H NMR for the sodium salt of the compound (400 MHz, D_2O, room temperature): δ 7.52 (d, 2H, J = 7.5 Hz), 7.40 (m, 4H), 7.35 (t, 2H, J = 7.5 Hz), 3.92 (d, 2H, J = 13.5 Hz), 3.81 (d, 2H, J = 13.5 Hz), 3.82 (d, 1H), 3.19 (d, 2H, J = 16.5 Hz), 3.10 (d, 2H, J = 16.5 Hz), 2.62 (d, 1H, J = 3.0 Hz), 2.60 (d, 1H, J = 3.0 Hz), 2.45 (d, 1H, J = 9.0 Hz), 2.40 (d, 1H, J = 9.0 Hz). ^{13}C NMR (400 MHz, D_2O, room temperature): δ 180.16, 178.81, 140.58, 134.40, 130.46, 128.51, 127.30, 126.39, 66.29, 58.70, 58.57, 56.72.

Synthesis of $Na_4[Cu_2Zn_2(ccdp)_2(\mu\text{-}OH)_2]\cdot CH_3OH\cdot 6H_2O$ (1). A methanol solution (10 mL) of ligand H_5ccdp (0.250 g, 0.457 mmol) and NaOH (0.128 g, 3.199 mmol) was slowly added at ambient temperature to a magnetically stirred solution of $Cu(ClO_4)_2\cdot 6H_2O$ (0.169 g, 0.457 mmol) and $Zn(ClO_4)_2\cdot 6H_2O$ (0.170 g, 0.457 mmol) in 15 mL of water during a period of 15 min. The whole reaction mixture was stirred at room temperature for 2 h. It was then filtered to discard any insoluble precipitates. The X-ray-quality sky-blue plate-shaped single crystals were obtained by slow ether diffusion into the clear filtrate after ∼15 days. Yield: 0.257 g (85%). Anal. Calcd for $C_{46}H_{44}N_4O_{20}Na_4Cu_2Zn_2$: C, 41.75; H, 3.33; N, 4.24; Cu, 9.61; Zn, 9.89. Found: C, 41.60; H, 3.53; N, 4.15; Cu, 9.71; Zn, 9.95. Molar conductance (MeOH): Λ_M = 392 Ω^{-1} cm^2 mol^{-1}. FTIR (KBr, cm^{-1}): ν 3436(b), 1607(s), 1589(s), 1563(s), 1452(s), 1387(vs), 1222(s), 1157(s), 1122(s), 1028(s), 996(s), 914(s),

dx.doi.org/10.1021/ic302099y | Inorg. Chem. 2013, 52, 2880−2890

759(s), 671(s). UV−vis (H_2O): λ_{max} (ε, L mol^{-1} cm^{-1}) = 760 (116), 270 (5771)^{sh}. MS (ESI): m/z 1265 (M^- = {[Cu_2Zn_2(ccdp)$_2$(μ-OH_2)$_2$]·CH_3OH + H}$^-$). μ_{eff} (total): 2.44 μ_B. μ_{eff}/Cu: 1.72 μ_B.

Synthesis of K_3[Cu_4(ccdp)$_2$(μ-OH)(μ-OH_2)]·14H_2O (2). To a solution of H_5ccdp (0.250 g, 0.457 mmol) and KOH (0.179g, 3.199 mmol) in methnol (10 mL) was added $Cu(ClO_4)_2$·$6H_2O$ (0.338 g, 0.914 mmol) in water (15 mL) with magnetic stirring during a period of 15 min. The reaction mixture was then stirred for 1 h, resulting in a greenish-blue solution. It was then filtered to discard any insoluble precipitates. The X-ray-quality blue plate-shaped single crystals were obtained by slow ether diffusion into the clear filtrate after ∼5 days. Yield: 0.269 g (88%). Anal. Calcd for $C_{46}H_{45}N_4O_{20}K_3Cu_4$: C, 41.07; H, 3.37; N, 4.16; Cu, 18.89. Found: C, 41.22; H, 3.80; N, 4.35; Cu, 18.97. Molar conductance (MeOH): Λ_M = 290 Ω^{-1} cm^2 mol^{-1}. FTIR (KBr, cm^{-1}): ν 3402(b), 1628(s), 1587(s), 1560(s), 1453(s), 1385(vs), 1220(s), 1152(s), 1112(s), 1031(s), 983(s), 923(s), 767(s), 715(s), 670(s). UV−vis (H_2O): λ_{max} (ε, L mol^{-1} cm^{-1}) = 763 (273), 266 (10825)^{sh}. MS (ESI): m/z 1294 (M^- = {[Cu_4(ccdp)$_2$(μ-OH_2)$_2$]·2CH_3OH + H}$^-$). μ_{eff} (total): 3.36 μ_B. μ_{eff}/Cu: 1.68 μ_B.

Caution! *Perchlorate salts of metal complexes are potentially explosive and should be handled in small quantities with great care.*

X-ray Crystallography and Data Analysis. Crystal data as well as data collection and refinement for complexes **1** and **2** are summarized in Table 1. Selected bond distances and bond angles are given in Table 2.

Table 1. Crystal Data and Structure Refinement for 1 and 2

	1	2
empirical formula	$C_{47}H_{60}N_4O_{27}Na_4Cu_2Zn_2$	$C_{46}H_{73}N_4O_{34}K_3Cu_4$
fw	1462.8	1597.6
cryst syst	triclinic	triclinic
space group	$P\bar{1}$	$P\bar{1}$
a, Å	14.0024(9)	13.9984(9)
b, Å	15.4647(9)	17.3764(12)
c, Å	17.0062(10)	18.4280(12)
α, deg	77.940(3)	109.399(4)
β, deg	68.504(3)	103.984(4)
γ, deg	64.402(3)	99.382(4)
volume, mm^3	3084.5(3)	3955.1(5)
Z	3	1
density (calcd), Mg/m^3	1.629	1.589
wavelength, Å	0.71073	0.71073
temperature, K	296	296
F(000)	1548	1857
abs coeff, mm^{-1}	1.568	1.826
θ range for data collection, deg	1.29−30.53	2.3−29.79
reflns collected	17818	17120
indep reflns	12181	11019
R1(F obsd data) [$I > 2\sigma(I)$]^a	0.0516	0.0697
wR2(F^2 all data)^b	0.1490	0.1949
GOF on F^2	1.035	0.997
largest diff peak and hole, e Å^{-3}	+2.173 and −1.524	+1.687 and −1.047

^{a}R1 = $\sum||F_o| - |F_c||/\sum|F_o|$. ^{b}wR2 = $\{\sum[w(F_o^2 - F_c^2)^2]/\sum[w(F_o^2)^2]\}^{1/2}$.

Clear sky-blue plate-shaped single crystals of complex **1** with approximate dimensions of 0.33 × 0.22 × 0.12 mm^3 and blue plate-shaped single crystals of complex **2** with approximate dimensions 0.6 × 0.4 × 0.2 mm^3 were selected for structural analysis. Intensity data for these compounds were collected using a diffractometer with a Bruker SMART CCD area detector[33] and graphite-monochromated Mo Kα radiation (λ = 0.71073 Å). For **1**, a total of 17818 data were measured with Miller indices h_{min} = −19, h_{max} = 17, k_{min} = −22, k_{max} = 21, l_{min} = −22, and l_{max} = 22 in the range 1.29 < θ < 30.53° using ω oscillation frames. The data were corrected for absorption by the multiscan method,[34] giving minimum and maximum transmission factors. The data were merged to form a set of 12181 independent reflections with R = 0.0516. The residual electron density is in the range +2.173 to −1.524 e Å^{-3}. For **2**, a total of 17120 data were recorded with Miller indices h_{min} = −17, h_{max} = 17, k_{min} = −22, k_{max} = 22, l_{min} = −23, and l_{max} = 23 in the range 1.24 < θ < 27.00° using ω oscillation frames. The data were corrected for absorption by the multiscan method,[34] giving minimum and maximum transmission factors. The data were merged to form a set of 11019 independent reflections with R = 0.0697. The residual electron density is in the range +1.687 to −1.047 e Å^{-3}. The structures were solved by direct methods and refined by full-matrix least-squares methods on F^2.[35] Hydrogen-atom positions were initially determined by geometry and refined by a riding model. Non-hydrogen atoms were refined with anisotropic displacement parameters. All hydrogen atoms were generated at ideal positions (C−H, 0.96 Å) and fixed with isotropic thermal parameters. In complex **1**, the solvent molecules, mainly diethyl ether molecules, show some disorder, but they could not be modeled to fit this space because some solvent molecules were lost during crystal handling.

DNA Binding Study. To investigate the DNA binding properties of complexes **1** and **2**, we titrated a fixed concentration of each complex (1 × 10^{-6} M) with varying concentrations of CT-DNA from 0 to 0.3 × 10^{-6} M, and the optical density was measured at 275 nm using UV−vis spectrophotometer [Shimadzu UV 1800 (190−1100 nm; 1 cm quartz cell)].

Protein Binding Study. We have studied the binding interactions of complexes **1** and **2** with BSA protein using standard Trp fluorescence with excitation at 280 nm and the corresponding emission at 339 nm, using a Perkin-Elmer-LS55 spectrofluorimeter equipped with *FLWINLAB* software with a rectangular quartz cuvette of 1 cm path length. A stock solution of BSA protein was prepared in phosphate buffer (pH ∼7.2). Concentrated stock solutions of complexes **1** and **2** were prepared by dissolving them separately in doubly distilled water and diluted suitably with doubly distilled water to get the required concentrations. An aqueous solution (2 mL) of BSA protein (0.375 × 10^{-6} M) was titrated by successive additions of the respective complexes [(0−11.285) × 10^{-5} M].

Theoretical Calculations. Theoretical calculations regarding structure optimization and the Fukui function (f_k^+) of the metal sites of the monomeric halves of complexes **1** and **2** were carried out with *Gaussian 03* software.[36] The functions f_k^+ were estimated from single-point calculations using the B3LYP[37] method and 6-311G[38] basis set at the optimized geometry, performed for N and N + 1 electron systems, where N is the total number of electrons in the system. In a finite difference approximation, f_k^+ of an atom k, in a molecule with N electrons, is expressed by the equation $f_k^+ = q_k(N) - q_k(N+1)$, where q_k is the charge of atom k.[39] The q_k values were calculated by Mulliken population analysis.

RESULTS AND DISCUSSION

Synthesis and General Characterization. The reaction of H_5ccdp with $Cu(ClO_4)_2$·$6H_2O$ and $Zn(ClO_4)_2$·$6H_2O$ in a 1:1:1 molar ratio in the presence of NaOH at pH ∼9 in methanol−water at room temperature in air led to the assembly of sky-blue heterometallic tetranuclear cluster **1** (Figure 2). The reaction of H_5ccdp with $Cu(ClO_4)_2$·$6H_2O$ in a 1:2 molar ratio in the presence of KOH at pH ∼9 in methanol−water at ambient temperature in air afforded a blue compound that was easily crystallized into a new tetranuclear cluster **2** (Figure 2). The molecular structures of complexes **1** and **2** have been established using a single-crystal X-ray diffraction study. Other analytical techniques used in the characterization of the complexes include elemental analysis, solution electrical conductivity, room temperature magnetic moment measurement, FTIR, UV−vis, high-field EPR, and MS techniques. The molar conductivity value of **1** in MeOH is 392 Ω^{-1} cm^2 mol^{-1} at room temperature, corresponding to a 4:1 electrolyte. Complex **2** behaves as a 3:1 electrolyte in a MeOH solution (Λ_M = 290 Ω^{-1} cm^2 mol^{-1}). The total room temperature magnetic moment value for **1** is 2.44 μ_B and that per each copper is 1.72 μ_B, indicating the presence of two Cu^{II} ions

dx.doi.org/10.1021/ic302099y | Inorg. Chem. 2013, 52, 2880−2890

Table 2. Selected Bond Lengths [Å] and Angles [deg] in 1 and 2

Bond Lengths			
1		2	
Zn1−O14	1.977(2)	Cu1−O5	1.889(4)
Zn1−O19	1.981(2)	Cu1−O1	1.987(4)
Zn1−O17	2.007(2)	Cu1−N4	1.992(5)
Zn1−O15	2.044(2)	Cu1−O8	2.069(4)
Zn1−N4	2.211(3)	Cu1−O18	2.178(4)
Zn2−O20	1.911(2)	Cu2−O4	1.926(4)
Zn2−O5	2.022(2)	Cu2−O1	1.960(4)
Zn2−O8	2.062(2)	Cu2−O2	1.996(4)
Zn2−O6	2.076(2)	Cu2−N3	2.016(6)
Zn2−N2	2.096(3)	Cu2−O25	2.237(4)
Cu1−O19	1.920(2)	Cu3−O4	1.911(4)
Cu1−O5	1.978(2)	Cu3−O10	1.982(4)
Cu1−O3	1.987(2)	Cu3−N1	2.020(5)
Cu1−N1	2.038(3)	Cu3−O15	2.069(4)
Cu1−O1	2.224(3)	Cu3−O12	2.084(5)
Cu2−O14	1.938(2)	Cu4−O5	1.885(4)
Cu2−O20	1.905(2)	Cu4−O10	1.956(4)
Cu2−O11	1.981(3)	Cu4−N2	1.991(5)
Cu2−N3	2.012(3)	Cu4−O11	2.002(4)
Cu2−O12	2.261(3)	Cu4−O7	2.259(4)
Bond Angles			
1		2	
O14−Zn1−O19	98.67(9)	O5−Cu1−O1	92.81(17)
O14−Zn1−O17	114.12(11)	O5−Cu1−N4	174.54(18)
O19−Zn1−O17	93.55(10)	O1−Cu1−N4	86.75(19)
O14−Zn1−O15	123.92(11)	O5−Cu1−O8	93.79(16)
O19−Zn1−O15	93.90(10)	O1−Cu1−O8	137.42(18)
O17−Zn1−O15	119.34(11)	N4−Cu1−O8	82.91(18)
O14−Zn1−N4	82.03(10)	O5−Cu1−O18	93.60(17)
O19−Zn1−N4	173.23(10)	O1−Cu1−O18	116.56(17)
O17−Zn1−N4	92.29(10)	N4−Cu1−O18	91.46(19)

Bond Angles			
1		2	
O15−Zn1−N4	80.23(10)	O8−Cu1−O18	104.93(16)
O20−Zn2−O5	93.73(10)	O4−Cu2−O1	96.52(18)
O20−Zn2−O8	100.26(10)	O4−Cu2−O2	93.39(18)
O5−Zn2−O8	103.35(10)	O1−Cu2−O2	161.51(18)
O20−Zn2−O6	94.06(10)	O4−Cu2−N3	175.11(18)
O5−Zn2−O6	139.95(11)	O1−Cu2−N3	85.66(19)
O8−Zn2−O6	113.73(10)	O2−Cu2−N3	83.4(2)
O20−Zn2−N2	168.77(11)	O4−Cu2−O25	91.05(17)
O5−Zn2−N2	83.83(10)	O1−Cu2−O25	99.69(16)
O8−Zn2−N2	90.97(11)	O2−Cu2−O25	95.68(16)
O6−Zn2−N2	81.05(10)	N3−Cu2−O25	92.89(18)
O19−Cu1−O5	96.85(10)	O4−Cu3−O10	96.74(17)
O19−Cu1−O3	91.10(10)	O4−Cu3−N1	177.06(19)
O5−Cu1−O3	157.06(11)	O10−Cu3−N1	85.30(19)
O19−Cu1−N1	173.51(10)	O4−Cu3−O15	88.02(17)
O5−Cu1−N1	86.55(10)	O10−Cu3−O15	117.00(17)
O3−Cu1−N1	83.73(11)	N1−Cu3−O15	92.95(19)
O19−Cu1−O1	95.63(9)	O4−Cu3−O12	95.63(18)
O5−Cu1−O1	97.23(10)	O10−Cu3−O12	122.9(2)
O3−Cu1−O1	103.38(10)	N1−Cu3−O12	81.5(2)
N1−Cu1−O1	89.40(10)	O15−Cu3−O12	118.9(2)
O20−Cu2−O14	98.52(10)	O5−Cu4−O10	95.19(18)
O20−Cu2−O11	89.67(11)	O5−Cu4−N2	172.66(19)
O14−Cu2−O11	163.34(12)	O10−Cu4−N2	86.5(2)
O20−Cu2−N3	172.73(11)	O5−Cu4−O11	93.07(18)
O14−Cu2−N3	86.19(11)	O10−Cu4−O11	165.80(17)
O11−Cu2−N3	84.40(12)	N2−Cu4−O11	83.9(2)
O20−Cu2−O12	90.04(10)	O5−Cu4−O7	91.96(17)
O14−Cu2−O12	105.53(11)	O10−Cu4−O7	98.07(17)
O11−Cu2−O12	88.84(11)	N2−Cu4−O7	94.90(19)
N3−Cu2−O12	94.05(11)	O11−Cu4−O7	93.16(17)

having one unpaired electron in each. The room temperature magnetic moment per copper for complex **2** is 1.68 μ_B, showing the presence of one unpaired electron in each Cu^{II} ion.

Description of the X-ray Crystal Structure of Complex 1. The crystal structure of complex **1** consists of a tetraanionic species $[Cu_2Zn_2(ccdp)_2(\mu\text{-}OH)_2]^{4-}$, four Na^+ ions along with a methanol, and six water molecules of crystallization. A structural view of the anion of complex **1** is shown in Figure 3. The tetraanionic species contains two Cu^{II} ions, two Zn^{II} ions, two $ccdp^{5-}$ ligands, and two OH^- ions. The heterotetranuclear complex anion is formed through the self-assembly of two $[CuZn(ccdp)]^-$ units exclusively bridged by two μ-OH^- groups. Each of the $[CuZn(ccdp)]^-$ units, contains a dinucleating $ccdp^{5-}$ ligand coordinated to the Cu^{II} and Zn^{II} centers. Both heterodinuclear units of the complex take similar structural arrangements with respect to the coordination mode of the $ccdp^{5-}$ ligand. Two aliphatic carboxylate arms and two aromatic carboxylate arms of the $ccdp^{5-}$ ligand in the complex are oriented in a trans fashion (Figure 4).

The respective metal centers in each of the heterodinuclear units pose different coordination geometries, bond lengths, and bond angles. For example, the coordination geometry around the Cu1 and Cu2 centers exhibit distorted square-pyramidal geometry, while the Zn1 and Zn2 centers exhibit distorted trigonal-bipyramidal geometry (Figure 5). Whereas the axial position of the square-pyramidal geometry around the Cu1 center is occupied by a benzoate oxygen atom of one $ccdp^{5-}$ ligand, the axial position around Cu2 is taken by a benzoate oxygen atom of the other $ccdp^{5-}$ ligand. The observed bond lengths for Cu1−O1 and Cu2−O12 are 2.224(3) and 2.261(3) Å, respectively. The square base of the pyramid around the Cu1 center is defined by the O3, O19, O5, and N1 atoms, whereas that around the Cu2 center is defined by the O11, O20, O14, and N3 atoms. The axial positions of a trigonal bipyramid around Zn1 are occupied by the tertiary amine nitrogen atom of the $ccdp^{5-}$ ligand and a bridging hydroxo (μ_2-OH) group with bond distances of Zn1−N4 = 2.211(3) Å and Zn1−O19 = 1.981(2) Å. Similarly, the axial positions around Zn2 are occupied by a tertiary amine nitrogen atom of the other $ccdp^{5-}$ ligand and the second bridging hydroxo (μ_2-OH) with bond distances of Zn2−N2 = 2.096(3) Å and Zn2−O20 = 1.911(2) Å. The triangular plane around the Zn1 center is defined by the O14, O15, and O17 atoms, whereas that around the Zn2 center is defined by the O5, O6, and O8 atoms. The distortion from the regular geometry around the Cu^{II} centers is more pronounced than the distortions observed around the Zn^{II} centers. This observation is consistent with the tendency that the Zn^{II} ion favors the trigonal-bipyramidal coordination geometry compared to the Cu^{II} ion.[40]

The average Cu---Zn separation in a dinuclear unit is 3.628 Å.[13a,19a,41] The average Cu---Zn separation where the copper and zinc centers are interligated to each other is 3.380 Å. The longer metal carboxylate arms with the shorter metal alkoxo arms provide the framework to support an average wide-bridging angle, Cu−O−Zn of 132.96°. The two different geometries observed within each heterodinuclear unit are due

dx.doi.org/10.1021/ic302099y | Inorg. Chem. 2013, 52, 2880−2890

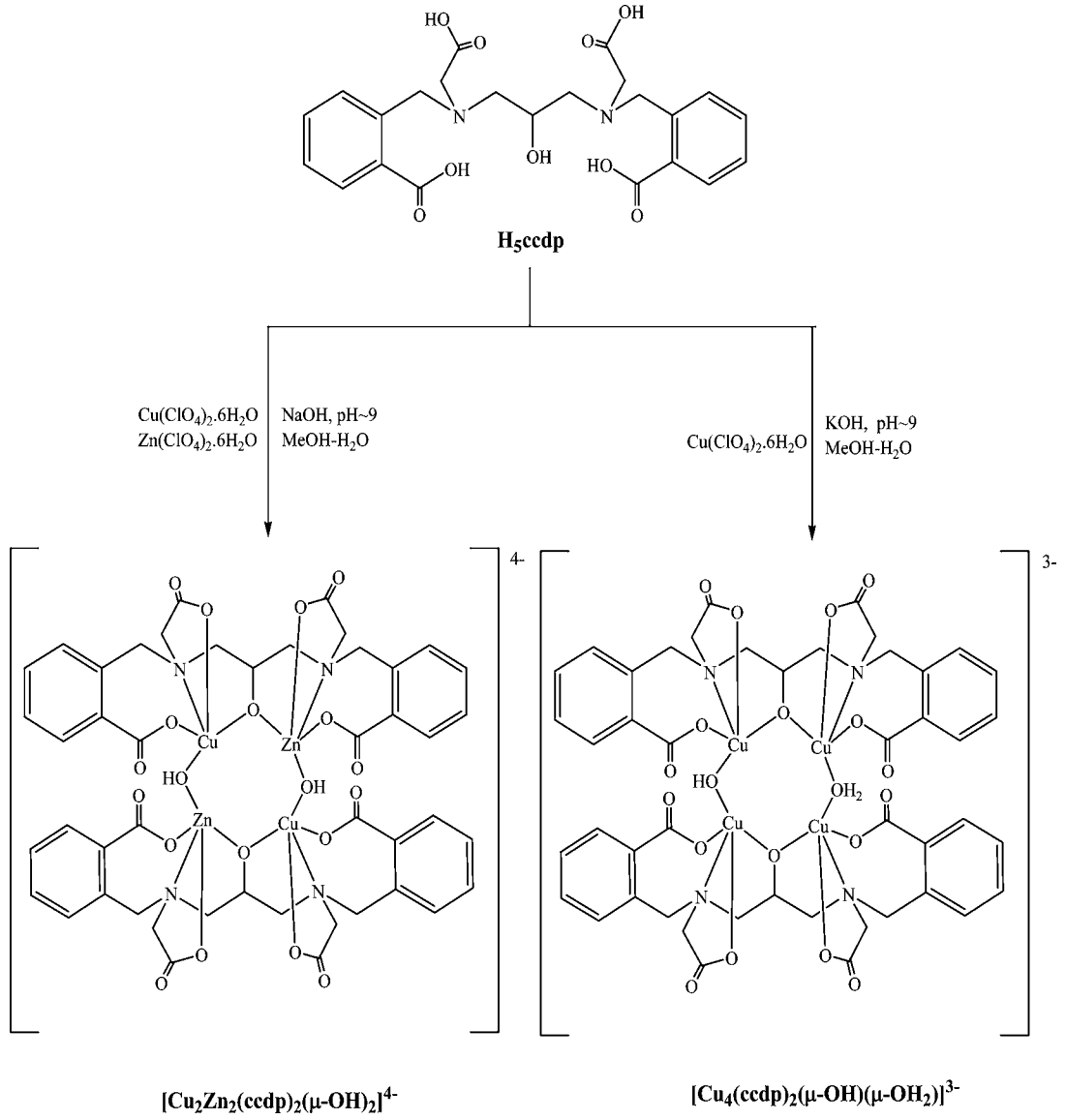

Figure 2. Synthetic procedure of complexes **1** and **2**.

to the different coordination modes adopted between the extremely flexible $ccdp^{5-}$ ligand and the metal ions in response to steric constraints within the complex. This strain has yielded a concave-shaped octagonal metal core defined by Zn1−O14−Cu2−O20−Zn2−O5−Cu1−O19, illustrated as part of Figure 5.

Interestingly, the solid-state X-ray crystal structure of complex **1** features a large number of ligand carboxylates and Na^{I} ions susceptible to being involved in a three-dimensional (3D) coordination network (Figure 6). In this network, the Na^{I} ions with their well-defined coordination environments join the two heterotetranuclear Cu_2Zn_2 units to form a heterooctanuclear Cu_4Zn_4 cluster (Figure S1 in the Supporting Information, SI). In this supramolecular arrangement, the repeating cluster consists of four Cu^{II}, four Zn^{II}, and eight Na^{I} metal ions.

Description of the X-ray Crystal Structure of Complex 2. A structural view of the tetranuclear Cu^{II} cluster anion of **2** is depicted in Figure 7. The crystal structure of the tetranuclear complex **2** consists of a trianionic species $[Cu_4(ccdp)_2(\mu\text{-OH})(\mu\text{-OH}_2)]^{3-}$ and three K^+ ions as countercations along with 14 water molecules of crystallization. This tetranuclear Cu^{II} cluster anion is formed through the self-assembly of two dinuclear $[Cu_2]$ pairs. The metal ions within each $[Cu_2]$ pair are bridged and chelated by one $ccdp^{5-}$ ligand. One hydroxyl group and one water molecule act as bridges between the two monoanionic dinuclear $[Cu_2(ccdp)]^-$ units through the Cu1−HO5−Cu4 and Cu2−H_2O4−Cu3 links, respectively. The Cu1−O5−Cu4 and Cu2−H_2O4−Cu3 bond angles of 122.33° and 127.60°, respectively, are open enough to afford further coordination by two oxygen atoms coming from one bridging OH^- group and one bridging H_2O molecule in a syn−syn bidentate fashion to the pair of Cu^{II} ions in each dinuclear unit. Within each dinuclear unit, the two aliphatic and two aromatic carboxylate arms of the $ccdp^{5-}$ ligand are oriented in a trans fashion (Figure 8).

The two copper centers in each dinuclear unit exhibit different coordination geometries, bond lengths, and bond angles. As shown in Figure 9, the Cu1 and Cu3 centers adopt distorted trigonal-bipyramidal geometry, whereas the Cu2 and Cu4 centers exhibit distorted square-pyramidal geometry. One bridging alkoxo oxygen, one monodentate aliphatic carboxylate oxygen, one monodentate aromatic carboxylate oxygen, one tertiary amine nitrogen of the $ccdp^{5-}$ ligand, and one bridging μ-OH^- group make up the coordination environment around the Cu1 and Cu4 centers.

dx.doi.org/10.1021/ic302099y | Inorg. Chem. 2013, 52, 2880−2890

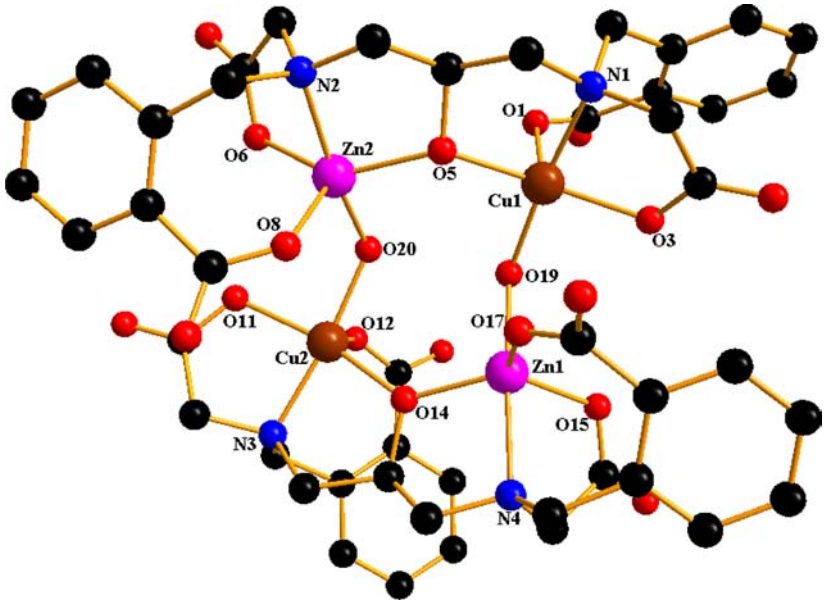

Figure 3. Molecular structure of complex **1** with an atom numbering scheme. Hydrogen atoms are omitted for clarity.

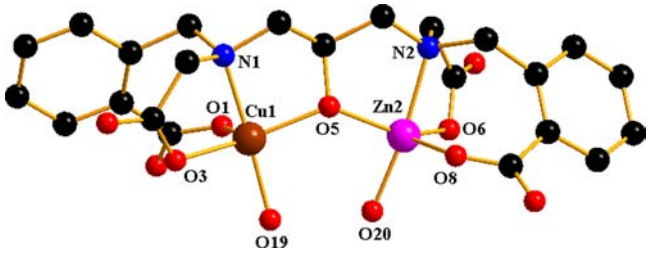

Figure 4. Molecular structure of the dinuclear unit of complex **1** with an atom numbering scheme showing the trans fashion of two aliphatic carboxylate arms and two aromatic carboxylate arms of the ligand.

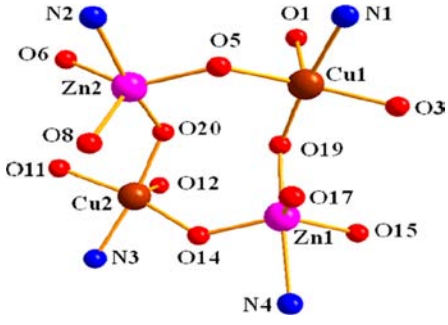

Figure 5. Core structure of complex **1** with an atom numbering scheme.

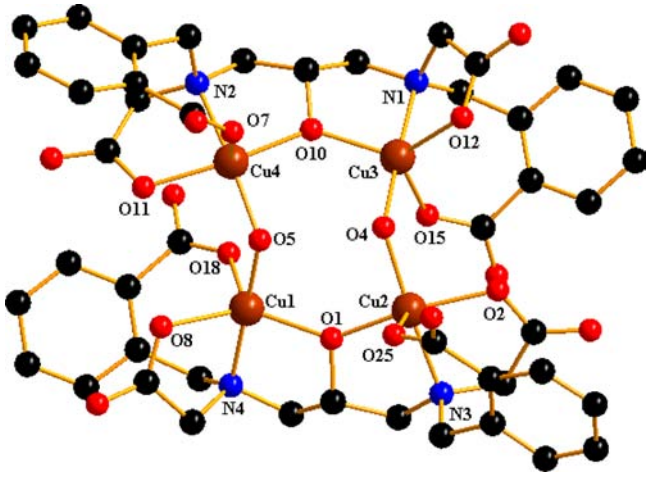

Figure 7. Molecular structure of complex **2** with an atom numbering scheme. Hydrogen atoms are omitted for clarity.

Similarly, one bridging alkoxo oxygen, one monodentate aliphatic carboxylate oxygen, one monodentate aromatic carboxylate oxygen, one tertiary amine nitrogen of the $ccdp^{5-}$ ligand, and one bridging μ-OH_2 molecule complete the coordination environment around the Cu2 and Cu3 centers. The two different coordination geometries observed within each dinuclear unit are due to the

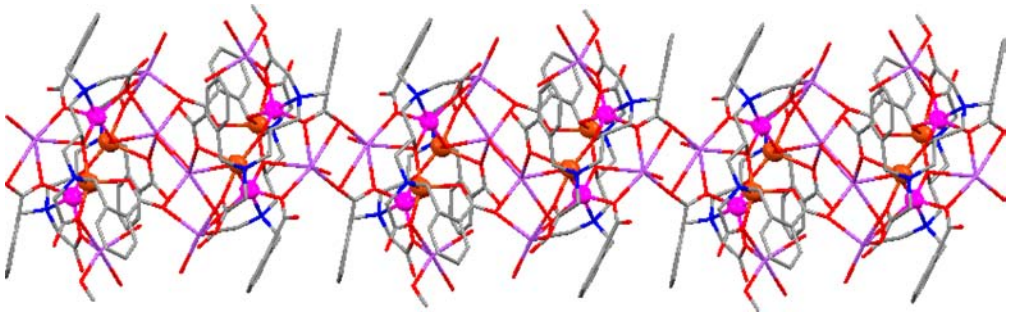

Figure 6. Stick representation of a 3D coordination network of **1**.

dx.doi.org/10.1021/ic302099y | *Inorg. Chem.* 2013, 52, 2880−2890

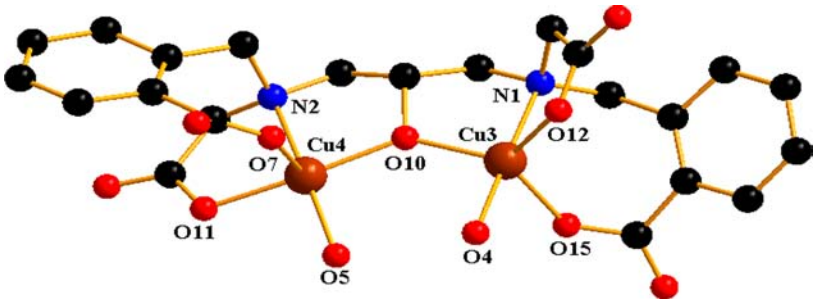

Figure 8. Molecular structure of the dinuclear unit of complex **2** with an atom numbering scheme showing the trans fashion of two aliphatic and two aromatic carboxylate arms of the ligand.

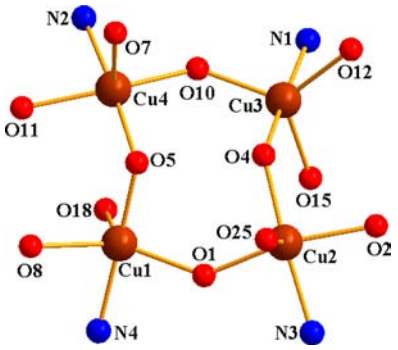

Figure 9. Core structure of complex **2** with an atom numbering scheme.

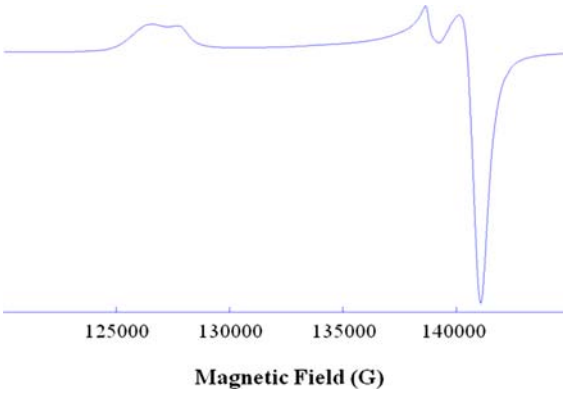

Figure 10. High-field (406.4 GHz) EPR spectrum of complex **1** at ca. 6 K.

different coordination modes adopted between the extremely flexible ccdp^{5-} ligand and the Cu^{II} ions in response to steric constraints within the complex. The coordination environment of the countercations K^+ may be best described by the distorted octahedral geometry, with either carboxylate and water/hydroxyl oxygen atoms or only water oxygen atoms. The Cu−O_{alkoxo} bond distances are within the range of previously reported alkoxo-bridged dinuclear copper systems.[42,43] The Cu−$O_{carboxylate}$ and Cu−N_{amine} bond distances are in the range of those previously reported in the literature.[42−46] The Cu−$O_{hydroxyl}$ bond distances (Cu1−O5 = 1.889 Å and Cu4−O5 = 1.886 Å) are quite shorter than the Cu−O_{water} bond distances (Cu2−O4 = 1.927 Å and Cu3−O4 = 1.910 Å). The Cu−O_{water} bond distances are comparable with the values reported in the literature.[47,48] The average Cu---Cu separation in a dinuclear unit is 3.679 Å. The average Cu---Cu separation where the two copper centers are interligated to each other is 3.375 Å. These bond distances are also in agreement with those reported in the literature.[49,50]

The crystal structures of complexes **1** and **2** exhibit a synergy with respect to the supramolecular assemblies. In complex **1**, two heterodinuclear $[CuZn(ccdp)]^-$ units are exclusively bridged by two μ-OH^- groups to form the heterotetranuclear cluster, whereas in complex **2**, two homodinuclear $[Cu_2(ccdp)]^-$ units are exclusively bridged by one μ-OH^- group and one μ-OH_2 molecule to form the homotetranuclear cluster. The main difference in their supramolecular structures is that complex **1** shows a 3D coordination network where the two heterotetranuclear Cu_2Zn_2 units are connected by the Na^I ions to form a heterooctanuclear Cu_4Zn_4 cluster, while complex **2** shows no 3D coordination network.

EPR and MS Studies. High-field (406.4 GHz) EPR spectra for complexes **1** and **2** in the powder state are collected at 6 K. The spectrum of complex **1** shows an isotropic signal consisting of hyperfine splitting patterns (Figure 10). The absence of seven hyperfine splitting lines (copper nuclear spin $I_{Cu} = {}^3/_2$) in the spectrum suggests the presence of magnetically isolated Cu^{II} centers in complex **1**. The spectrum shows the splitting between the lines in both the low- and high-field pairs scales with the microwave frequency, which suggests that there are no zero-field-splitting effects. This might be due to the broadening of the ligand hyperfine splitting. The spectrum shows the superposition of two spectra from two essentially isolated magnetically inequivalent sites for Cu^{II} ions. One copper center has $g_x = g_y = 2.061$, and $g_z = 2.294$, and the other copper center has $g_x = 2.085$, $g_y = 2.092$, and $g_z = 2.274$. These parameters are very weakly dependent on the temperature. Thus, no coupling interactions in complex **1**, where the two Cu^{II} centers occupy opposite corners of the core and are not directly bridged to each other, are observed. The spectrum of complex **2** is very weak at room temperature but becomes stronger at lower temperature and persists as strong down to 6 K (Figure S2 in the SI). The spectrum could be interpreted in terms of a mononuclear copper(II) complex. Additionally, the presence of the spectral features in the low field is due to hyperfine splitting of the Cu^{II} signal by a coordinated nitrogen atom. The spectrum has resolved g values of $g_x = g_y = 2.060$ and $g_z = 2.264$, which are typical for copper(II) complexes, either mono- or mulitinuclear with at least one noninteracting copper atom.[51,52]

In an attempt to further characterize complexes **1** and **2**, methanolic solutions (pH ∼7.5) were negative-ion electrosprayed into a quadrupole ion-trap mass spectrometer and subjected to collision-induced dissociation to gain structural information. The MS spectrum of complex **1** (Figure S3 in the SI) shows a signal at m/z 1265, which corresponds to the $\{[Cu_2Zn_2(ccdp)_2(\mu\text{-}OH_2)_2]\cdot CH_3OH + H\}^-$ species, reconfirming the heterodimetallic nature of complex **1** even in solution. The MS spectrum of complex **2** yields a signal at m/z 1294, which

dx.doi.org/10.1021/ic302099y | Inorg. Chem. 2013, 52, 2880−2890

corresponds to the $\{[Cu_4(ccdp)_2(\mu\text{-}OH_2)_2]\cdot 2CH_3OH + H\}^-$ species, confirming the homodimetallic nature of complex **2** in solution. Therefore, the mass spectral analyses suggest that both the hetero- and homodimetallic tetranuclear complexes are stable in solution at physiological pH.

Binding Studies. Complexes **1** and **2** are highly water-soluble and well-stable in solution at physiological pH. So, considering that copper and zinc ions and their complexes in biological systems may act as biological probes, we were interested in investigating their DNA and protein binding affinity in an aqueous medium. Accordingly, we have performed UV−vis and fluorescence experiments to evaluate their binding interactions with DNA and BSA protein.

Binding of Complexes 1 and 2 with DNA. We have observed from UV−vis experiments that complexes **1** and **2** do not interact with DNA because there are no changes of the absorption maxima of the complexes upon the addition of CT-DNA. The representative UV−vis spectra for complex **1** in the absence of CT-DNA and in the presence of CT-DNA are shown in Figure S4 in the SI.

Binding of Complexes 1 and 2 with BSA Protein. Because BSA constitutes ~55% of the total protein in blood plasma and it plays an important role in drug transport and drug metabolism, the interactions of complexes **1** and **2** with BSA have been studied from the binding experiments with BSA as a model protein. The binding of complexes with BSA protein in an aqueous medium has been investigated from the concentration dependence of the change in the fluorescence intensity of protein upon the addition of complexes. A BSA molecule consists of three aromatic amino acids (phenylalanine, tyrosine, and tryptophan), and its fluorescence can appear because of tryptophan and tyrosine residues.[53] Figure 11 shows the effect of complex **1** on the fluorescence intensity of BSA

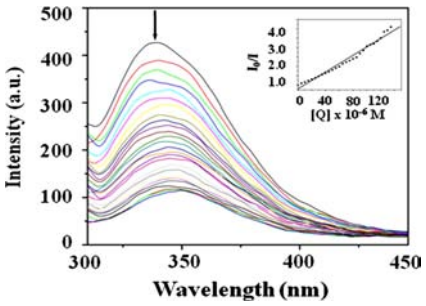

Figure 11. Emission spectra of BSA protein in an aqueous medium (0.375×10^{-6} M; λ_{exi} = 280 nm; λ_{emi} = 339 nm) as a function of the concentration of complex **1** [(0−11.285) × 10^{-5} M]. Inset: Stern−Volmer plot of the fluorescence titration data. The arrow indicates the change in the emission intensity with respect to various concentrations of complex **1**.

protein in water. Upon increasing concentration of complex **1**, a gradual decrease in the fluorescence intensity accompanied by a significant red shift has been observed. Following the same procedure, the fluorescence titration experiments of BSA protein with complex **2** have been executed. The fluorescence spectra indicate that there is a progressive decrease in the fluorescence intensity along with a significant red shift (Figure 12). This quenching effect with an observed red shift indicates the interaction of BSA protein with the title complexes.[23b,54] The mechanisms of quenching are usually classified by either dynamic quenching or static quenching. Static quenching refers to

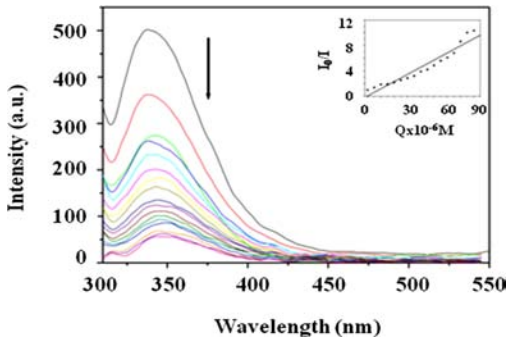

Figure 12. Emission spectra of BSA protein in an aqueous medium (0.375×10^{-6} M; λ_{exi} = 280 nm; λ_{emi} = 339 nm) as a function of the concentration of complex **2** [(0−11.285) × 10^{-5} M]. Inset: Stern−Volmer plot of the fluorescence titration data. The arrow indicates the change in the emission intensity with respect to various concentrations of complex **2**.

fluorophore−quencher complex formation, and the dynamic quenching refers to a process in which the fluorophore and quencher come into contact during the transient existence of the excited state. The fluorescence quenching data have been analyzed by the Stern−Volmer relation $I_0/I = 1 + K_{SV}[Q]$, where I_0 and I are the fluorescence intensities of the fluorophore in the absence and presence of quencher, respectively, K_{SV} is the Stern−Volmer quenching constant, and [Q] is the quencher concentration. A plot of I_0/I versus [Q] with respect to complexes **1** and **2** results in a linear graph, and the K_{SV} values are calculated from the slope. The Stern−Volmer plots of the fluorescence titration data for complexes **1** and **2** are shown in Figures 11 and 12, inset. Because the lifetime of BSA protein is on the order of 10^{-9} s, the calculated bimolecular quenching rate constants (k_q) using $K_{SV} = k_q\tau_0$ were found to be higher than the maximum collisional quenching (k_q) of various kinds of quenchers to biopolymers (2.0×10^{10} M^{-1} s^{-1}). Hence, fluorescence quenching results from the formation of a Cu_2Zn_2-BSA complex/Cu_4-BSA complex.

At a certain point, when small molecules bind independently to a set of equivalent sites on a macromolecule, some will be in bound condition and some will be in unbound condition. So, the equilibrium between the unbound and bound molecules is represented by the Scatchard equation[55,56] $\log[(F_0 - F)/F] = \log(K) + n \log [Q]$, where K and n are the binding constant and the number of binding sites, respectively, and F_0 and F are the fluorescence intensities in the absence and presence of the quencher, respectively. Thus, a plot of $\log(F_0 - F)/F$ versus log

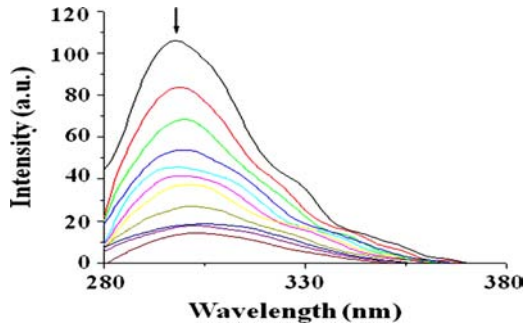

Figure 13. Synchronous fluorescence spectra of BSA (0.375×10^{-6} M) as a function of the concentration of complex **1** [(0−11.285) × 10^{-5} M] with a wavelength difference of $\Delta\lambda$ = 15 nm. The arrow indicates the change in the emission intensity with respect to various concentrations of complex **1**.

dx.doi.org/10.1021/ic302099y | Inorg. Chem. 2013, 52, 2880−2890

[Q] (Figures S5 and S6 in the SI) can be used to determine the value of the binding constants, and such values were calculated to be 4.669×10^4 and 3.562×10^5 M^{-1} for complexes **1** and **2**, respectively. From the value of the binding constants, it can be suggested that complex **2** interacts more strongly with BSA protein compared to that of complex **1** under the physiological condition. The difference in the binding strength between complexes **1** and **2** is most likely due to variation of the Cu^{II} and Zn^{II} ions in the respective complexes. The binding strengths of complexes **1** and **2** are comparable to those of the reported mononuclear copper(II), nickel(II), cobalt(II), and gadolineum-(III) complexes in the literature.[57−59] Because complexes **1** and **2** are tetranuclear clusters, their binding constant values could be lesser attributed to the steric effects arising out of the number of acetate and benzoate functionalities of the ligand. However, surprisingly, the complexes show comparably high BSA binding propensity in an aqueous medium at pH ∼7.2, possibly because of the additional hydrogen-bonding ability of the acetate and benzoate groups with the peptide backbone.

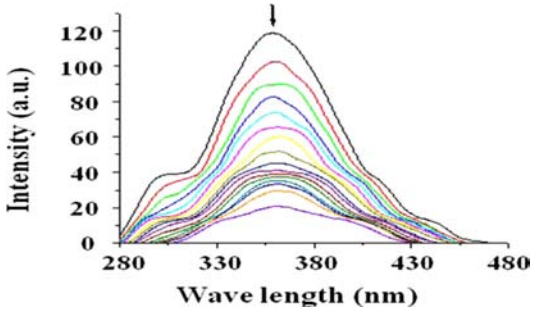

Figure 14. Synchronous fluorescence spectra of BSA (0.375×10^{-6} M) as a function of the concentration of complex **1** [$(0-11.285) \times 10^{-5}$ M] with a wavelength difference of $\Delta\lambda$ = 60 nm. The arrow indicates the change in the emission intensity with respect to various concentrations of complex **1**.

Table 3. Fukui Functions of the Monomeric Analogues (1m and 2m) of Complexes 1 and 2

	1m		2m	
	Cu	Zn	Cu	Cu
f_k^+	0.1539	0.0034	0.1276	0.0503

In synchronous fluorescence spectroscopy, according to Miller,[60] the difference between excitation and emission wavelengths ($\Delta\lambda = \lambda_{emi} - \lambda_{exc}$) reflects the spectra of a different nature of chromophores. With large $\Delta\lambda$ values such as 60 nm, the synchronous fluorescence of BSA is characteristic of the tryptophan residue, and with a small $\Delta\lambda$ value, such as 15 nm, it is characteristic of tyrosine.[61] To understand the structural changes of BSA protein due to the addition of complexes **1** and **2**, we have measured synchronous fluorescence spectra of the former with respect to the addition of test complexes. At $\Delta\lambda$ = 15 nm, the intensity of emission at 303 nm corresponding to tyrosine was found to decrease significantly upon increasing concentrations of complexes **1** and **2** with a red shift of the emission wavelength (Figures 13 and S7 in the SI). However, at $\Delta\lambda$ = 60 nm, the tryptophan fluorescence showed a significant decrease in the intensity of emission (at 360 nm) without any change in the position of the emission band (Figures 14 and S8 in the SI). The results indicate that the microenvironments of both tyrosine and tryptophan residues in BSA have been affected by the complexes during the binding process, highlighing that the effect is more pronounced toward tyrosine than tryptophan. Hence, the results clearly indicate that complexes **1** and **2** bind to active sites in the protein, which make them potential molecules for biological applications. These results are comparable with earlier literature reports.[62]

Density Functional Theory (DFT) Calculations. In order to gain a better understanding of where the complexes bind to BSA protein, we have carried out DFT calculations. Calculations have been performed on the monomeric halves $[Cu^{II}Zn^{II}(ccdp)(OH)_2]^{3-}$ (**1m**) and $[Cu_2^{II}(ccdp)(OH)(OH_2)]^{2-}$ (**2m**) of

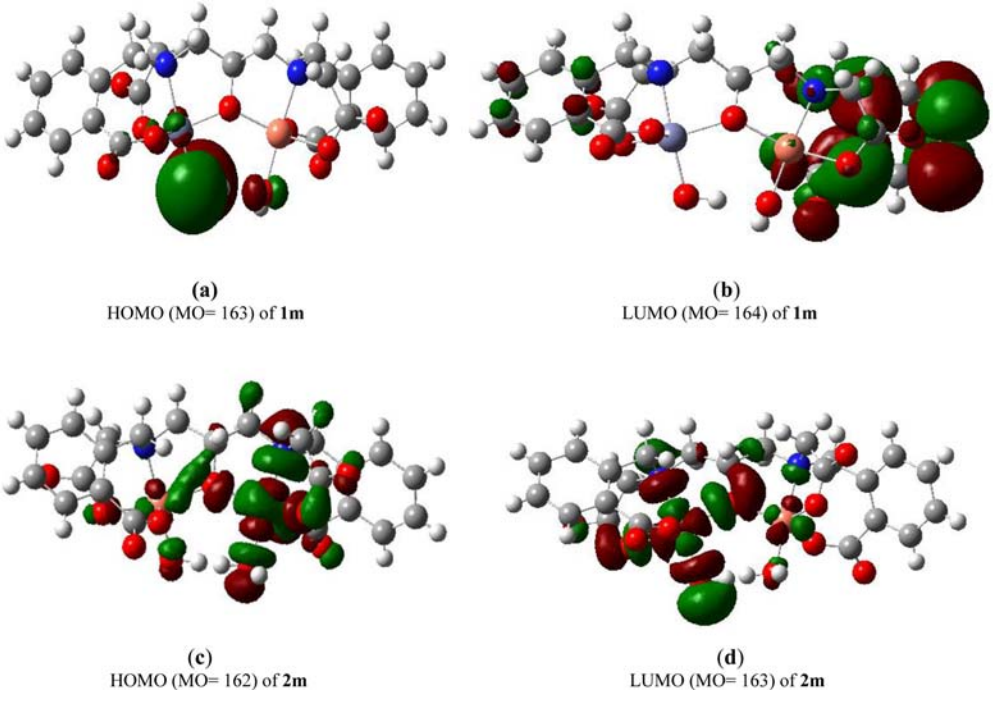

Figure 15. Representative HOMOs and LUMOs of monomeric analogues of complexes **1** and **2** calculated at the B3LYP/[6-311G] level of theory.

dx.doi.org/10.1021/ic302099y | Inorg. Chem. 2013, 52, 2880−2890

representative complexes **1** and **2** and on the corresponding one-electron-reduced analogues $\mathbf{1m}^-$ and $\mathbf{2m}^-$ at the B3LYP level using the *Gaussian 03* software package. The structures of **1m** and **2m** proved to be the doublet ground state ($S = {}^1/_2$) and the closed-shell singlet state, respectively, with optimized structural parameters fully consistent with crystallographic data. The one-electron-reduced species $\mathbf{1m}^-$ and $\mathbf{2m}^-$ display a closed-shell singlet state and a doublet ($S = {}^1/_2$) ground state, respectively. The calculated condensed Fukui function values f_k^+ at the metal sites of the monomeric halves are given in Table 3. According to the values presented in Table 3, it can be anticipated that BSA protein binds as a nucleophile to the copper centers ($f_k^+ = 0.1539$) more favorably than zinc centers ($f_k^+ = 0.0034$) in complex **1**. In complex **2**, the Fukui function values of all of the copper centers are fairly close in magnitude, and thereby it is presumed that the BSA protein may interact with all of the copper centers with more or less equal probability. The small difference in the Fukui function values at the two copper sites is most likely due to the different coordination geometries around the two copper centers in the monomeric half of complex **2**. In **1m**, while the highest occupied molecular orbital (HOMO) is located near the zinc center, the lowest unoccupied molecular orbital (LUMO) is spread on and around the copper center (Figure 15a,b). Therefore, the BSA protein being a nucleophile will prefer to interact with the copper center more preferably. This is in accordance with the findings observed in Fukui function calculations. In the one-electron-reduced analogue $\mathbf{1m}^-$, the HOMOs and LUMOs are spread mostly on and around the copper center rather than the zinc center (Figure S9a,b in the SI). The HOMOs and LUMOs in **2m** are spread on and around both copper centers, indicating the involvement of all of the copper centers in the binding process with BSA protein (Figure 15c,d). Generally, the Cu^{II} ion is known as the fluorescence quencher.[63,64] Recently, it has also been reported that the fluorescence emission of BSA protein and other substrates has significantly been quenched because of interaction with Cu^{II} ions.[63−65] Therefore, DFT calculation results strongly suggest that the binding of BSA protein with complexes **1** and **2** occurs more possibly through the copper centers, which has been further supported by the fluorescence titration experiments involving a significant quenching effect.

CONCLUSIONS

In conclusion, we have described the preparation and characterization of two new water-soluble hetero- and homometallic tetranuclear clusters, $Cu_2^{II}Zn_2^{II}$ and Cu_4^{II}, using a symmetrical carboxylate-rich dinucleating ligand. The high-field EPR spectral analysis reveals that there are no exchange interactions between the Cu^{II} ions in cluster **1**, while in complex **2**, there is at least one noninteracting Cu^{II} center coordinated to a nitrogen atom. The complexes show evidence of binding with BSA protein in an aqueous medium at physiological pH indicating the significance of designing new water-soluble polynuclear transition-metal complexes based on carboxylate-rich ligands to be used as potential binding agents to different biological macromolecules and subsequent metal-based drugs. These hetero- and homotetranuclear clusters **1** and **2** aim at combining the advantages of structural control and diversity attained within supramolecular edifices, with properties arising due to different metal ions sitting in close proximity to polynuclear assemblies having biological implications.

ASSOCIATED CONTENT

Supporting Information

X-ray crystallographic data in CIF format for complexes **1** and **2**, experimental details of the ligand and its synthetic scheme, MS spectra of the complexes, EPR, electronic spectra, Scatchard plots, synchronous fluorescence spectra, and HOMO and LUMO. This material is available free of charge via the Internet at http://pubs.acs.org.

AUTHOR INFORMATION

Corresponding Author

*E-mail: mbera2009@klyuniv.ac.in (M.B.), ghezai.musie@utsa.edu (G.T.M.). Fax: +91 33 25828282. Tel: +91 33 25828282 x306.

Notes

The authors declare no competing financial interest.

ACKNOWLEDGMENTS

The authors thank the Department of Science and Technology (DST; Grant SR/FT/CS-067/2009), New Delhi, for funding and financial support. The authors acknowledge Prof. Andrew Ozarowski, National High Magnetic Field Laboratory, Florida State University, for measurement of the high-frequency EPR spectra. The instrumental facilities provided by the DST-FIST, DST-PURSE and UGC-SAP program in the Department of Chemistry are greatly acknowledged. A.P. also thanks the University of Kalyani for providing a university research fellowship.

REFERENCES

(1) Rosenzweig, A. C.; Frederick, C. A.; Lippard, S. J.; Nordlund, P. *Nature* **1993**, *366*, 537.
(2) Whittington, D. A.; Lippard, S. J. *J. Am. Chem. Soc.* **2001**, *123*, 827.
(3) Jabri, E.; Carr, M. B.; Hausinger, R. P.; Karplus, P. A. *Science* **1995**, *268*, 998.
(4) Gerdemann, C.; Eicken, C.; Krebs, B. *Acc. Chem. Res.* **2002**, *35*, 183.
(5) Khanra, S.; Weyhermuller, T.; Bill, E.; Chaudhuri, P. *Inorg. Chem.* **2006**, *45*, 5911.
(6) Ueki, S.; Kobayashi, Y.; Ishida, T.; Nogami, T. *Chem. Commun.* **2005**, 5223.
(7) Kornienko, A.; Banerjee, S.; Kumar, G. A.; Riman, R. E.; Emge, T. J.; Brennan, J. G. *J. Am. Chem. Soc.* **2005**, *127*, 14008.
(8) Sadhukhan, N.; Bera, J. K. *Inorg. Chem.* **2009**, *48*, 978.
(9) Gianneschi, N. C.; Masar, M. S.; Mirkin, C. A. *Acc. Chem. Res.* **2005**, *38*, 825.
(10) Mandal, S. K.; Roesky, H. W. *Acc. Chem. Res.* **2010**, *43*, 248.
(11) Mukherjee, A.; Nembenna, S.; Sen, T. K.; Sarish, S. P.; Ghorai, P. K.; Ott, H.; Stalke, D.; Mandal, S. K.; Roesky, H. W. *Angew. Chem., Int. Ed.* **2011**, *50*, 3968.
(12) Kahn, O. *Magnetism:A Supramolecular Function*; NATO ASI Series C; Kluwer Academic Publishers: Dordrecht, The Netherlands, 1996; Vol. *484*.
(13) (a) Roth, A.; Spielberg, E. T.; Plass, W. *Inorg. Chem.* **2007**, *46*, 4362. (b) Ghosh, D.; Kundu, N.; Maity, G.; Choi, K. Y.; Cane-schi, A.; Endo, A.; Chaudhury, M. *Inorg. Chem.* **2004**, *43*, 6015.
(14) Dongfeng, L.; Shuan, L.; Dexi, Y.; Jiuhong, Y.; Jin, H.; Yizhi, L.; Wenxia, T. *Inorg. Chem.* **2003**, *42*, 6071.
(15) Mukhopadhyay, U.; Govindasamy, L.; Ravikumar, K.; Velmurugan, D.; Ray, D. *Inorg. Chem. Commun.* **1998**, *1*, 152.
(16) Torelli, S.; Belle, C.; Gautier-Luneau, I.; Hamman, S.; Pierre, J.-L. *Inorg. Chim. Acta* **2002**, *333*, 144.
(17) Gao, J.; Reibenspies, J. H.; Martell, A. E. *Angew. Chem., Int. Ed.* **2003**, *42*, 6008.

(18) Paschke, R.; Liebsch, S.; Tschierske, C.; Oakley, M. A.; Sinn, E. *Inorg. Chem.* **2003**, *42*, 8230.
(19) (a) Buvaylo, E. A.; Kokozay, V. N.; Vassilyeva, O. Y.; Skelton, B. W.; Jezierska, J.; Brunel, L. C.; Ozarowski, A. *Chem. Commun.* **2005**, 4976. (b) Osa, S.; Sunatsuki, Y.; Yamamoto, Y.; Nakamura, M.; Shimamoto, T.; Matsumoto, N.; Re, N. *Inorg. Chem.* **2003**, *42*, 5507. (c) Nakamura, Y.; Yonemura, M.; Arimura, K.; Usuki, N.; Ohba, M.; Okawa, H. *Inorg. Chem.* **2001**, *40*, 3739.
(20) Stewart, A. J.; Blindauer, C. A.; Berezenko, S.; Sleep, D.; Sadler, P. J. *Proc. Natl. Acad. Sci. U.S.A.* **2003**, *100*, 3701.
(21) Masuoka, J.; Hegenauer, J.; Van Dyke, B. R.; Saltman, P. *J. Biol. Chem.* **1993**, *268*, 21533.
(22) Stryer, L. *Biochemistry*, 4th ed.; Freeman: New York, 1995.
(23) (a) Saha, S.; Mallick, D.; Majumdar, M. R.; Dighe, R. R.; Jemmis, E. D.; Chakravarty, A. R. *Inorg. Chem.* **2011**, *50*, 2975. (b) Sathyadevi, P.; Krishnamoorthy, P.; Alagesan, M.; Thanigaimani, K.; Muthiah, P. T.; Dharmaraj, N. *Polyhedron* **2012**, *31*, 294.
(24) Humphreys, K. J.; Karlin, K. D.; Rokita, S. E. *J. Am. Chem. Soc.* **2002**, *124*, 8055.
(25) (a) Montero, E. I.; Benedetti, J. B.; Mangrum, M. J.; Oehlsen, Y. Q.; Farrell, N. P. *Dalton Trans.* **2007**, 4938. (b) Mandal, D.; Chauhan, M.; Arjmand, F.; Aromi, G.; Ray, D. *Dalton Trans.* **2009**, 9183.
(26) Carlsson, H.; Haukka, H.; Bousseksou, A.; Latour, J. M.; Nordlander, E. *Inorg. Chem.* **2004**, *43*, 8252.
(27) Bera, M.; Musie, G. T.; Powell, D. R. *Inorg. Chem.* **2009**, *48*, 4625.
(28) Curtiss, A. B. S.; Bera, M.; Musie, G. T.; Powell, D. R. *Dalton Trans.* **2008**, 2717.
(29) Bera, M.; Musie, G. T.; Powell, D. R. *Inorg. Chem. Commun.* **2010**, *13*, 1029.
(30) Patra, A.; Sen, T. K.; Bhattacharyya, R.; Mandal, S. K.; Bera, M. *RSC Adv.* **2012**, *2*, 1774.
(31) Carlin, R. L. *Magnetochemistry*; Springer-Verlag: New York, 1986.
(32) Hassan, A. K.; Pardi, L. A.; Krzystek, J.; Sienkiewicz, A.; Goy, P.; Rohrer, M.; Brunel, L. C. *J. Magn. Reson.* **2000**, *142*, 300.
(33) (a) Data Collection: *SMART Software Reference Manual*, Bruker-AXS: Madison, WI, 1998. (b) Data Reduction: *SAINT Software Reference Manual*; Bruker-AXS: Madison, WI, 1998.
(34) Sheldrick, G. M. *SADABS. Program for Multi-Scan Absorption Correction of Area Detector Data*; University of Göttingen: Göttingen, Germany, 2002.
(35) (a) Sheldrick, G. M. *SHELXTL; Version 6.10 Reference Manual*; Bruker AXS: Madison, WI, 2000. (b) *International Tables for Crystallography*; Kluwer: Boston, MA, 1995; Vol. *C*, Tables 6.1.1.4, 4.2.6.8, and 4.2.4.2.
(36) Frisch, M. J.; Trucks, G. W.; Schlegel, H. B.; Scuseria, G. E.; Robb, M. A.; Cheeseman, J. R.; Montgomery, J. A., Jr.; Vreven, T.; Kudin, K. N.; Burant, J. C.; Millam, J. M.; Iyengar, S. S.; Tomasi, J.; Barone, V.; Mennucci, B.; Cossi, M.; Scalmani, G.; Rega, N.; Petersson, G. A.; Nakatsuji, H.; Hada, M.; Ehara, M.; Toyota, K.; Fukuda, R.; Hasegawa, J.; Ishida, M.; Nakajima, T.; Honda, Y.; Kitao, O.; Nakai, H.; Klene, M.; Li, X.; Knox, J. E.; Hratchian, H. P.; Cross, J. B.; Adamo, C.; Jaramillo, J.; Gomperts, R.; Stratmann, R. E.; Yazyev, O.; Austin, A. J.; Cammi, R.; Pomelli, C.; Ochterski, J. W.; Ayala, P. Y.; Morokuma, K.; Voth, G. A.; Salvador, P.; Dannenberg, J. J.; Zakrzewski, V. G.; Dapprich, S.; Daniels, A. D.; Strain, M. C.; Farkas, O.; Malick, D. K.; Rabuck, A. D.; Raghavachari, K.; Foresman, J. B.; Ortiz, J. V.; Cui, Q.; Baboul, A. G.; Clifford, S.; Cioslowski, J.; Stefanov, B. B.; Liu, G.; Liashenko, A.; Piskorz, P.; Komaromi, I.; Martin, R. L.; Fox, D. J.; Keith, T.; Al-Laham, M. A.; Peng, C. Y.; Nanayakkara, A.; Challacombe, M.; Gill, P. M. W.; Johnson, B.; Chen, W.; Wong, M. W.; Gonzalez, C.; Pople, J. A. *Gaussian 03*, revision A.1; Gaussian, Inc.: Pittsburgh, PA, 2003.
(37) (a) Becke, A. D. *Phys. Rev. A* **1988**, *38*, 3098. (b) Lee, C.; Yang, W.; Parr, R. G. *Phys. Rev. B* **1988**, *37*, 785.
(38) Ditchfield, R.; Hehre, W. J.; Pople, J. A. *J. Chem. Phys.* **1971**, *54*, 724.
(39) Yang, W.; Mortier, W. J. *J. Am. Chem. Soc.* **1986**, *108*, 5708.
(40) Ohtsu, H.; Shimazaki, Y.; Odani, A.; Yamauchi, O.; Mori, W.; Itoh, S.; Fukuzumi, S. *J. Am. Chem. Soc.* **2000**, *122*, 5733.
(41) Nakamura, Y.; Yonemura, M.; Arimura, K.; Usuki, N.; Ohba, M.; Okawa, H. *Inorg. Chem.* **2001**, *40*, 3739.
(42) Lai, T. C.; Chen, W. H.; Lee, C. J.; Wang, B. C.; Wei, H. H. *J. Mol. Struct.* **2009**, *935*, 97.
(43) Seppala, P.; Colacio, E.; Mota, A. J.; Sillanpaa, R. *Inorg. Chim. Acta* **2010**, *363*, 755.
(44) Fielden, J.; Sprott, J.; Long, D.-L.; Kogerler, P.; Cronin, L. *Inorg. Chem.* **2006**, *45*, 2886.
(45) Belousoff, M. J.; Graham, B.; Spiccia, L. *Eur. J. Inorg. Chem.* **2008**, 4133.
(46) (a) Wang, L.; Wang, J.; Xie, C. *J. Coord. Chem.* **2008**, 3401. (b) Chandrasekhar, V.; Senepati, T.; Dey, A.; Sanudo, E. C. *Inorg. Chem.* **2011**, *50*, 1420.
(47) Korabik, M.; Materny, M.; Surga, W.; Glowiak, T.; Mrozinski, J. *J. Mol. Struct.* **1998**, *443*, 255.
(48) Caballero, A. B.; Rodríguez-Diéguez, A.; Lezama, L.; Salas, J. M. *Cryst. Growth Des.* **2012**, *12*, 3583.
(49) Jabri, E.; Carr, M. B.; Hausinger, R. P.; Karplus, P. A. *Science* **1995**, *268*, 998.
(50) Kim, M. H.; Choi, W.-C.; Kang, H. O.; Lee, J. S.; Kang, B. S.; Kim, K.-J.; Derewenda, Z. S.; Oh, T.-K.; Lee, C. H.; Lee, J.-K. *Proc. Natl. Acad. Sci. U.S.A.* **2005**, *49*, 17606.
(51) Owen, S. J. T.; Standley, K. J.; Walker, A. *J. Chem. Phys.* **1964**, *40*, 183.
(52) Roberts, E. M.; Koski, W. S. *J. Am. Chem. Soc.* **1961**, *83*, 1865.
(53) Osama, K. A. Z.; Othman, I. K. A. S. *J. Am. Chem. Soc.* **2008**, *130*, 10793.
(54) Wang, Q.; Lu, L.; Yuan, C.; Pei, K.; Liu, Z.; Guo, M.; Zhu, M. *Chem. Commun.* **2010**, *46*, 3547.
(55) Lakowicz, J. R. *Fluorescence Quenching: Theory and Applications. Principles of Fluorescence Spectroscopy*; Kluwer Academic/Plenum Publishers: New York, 1999; pp 53−127.
(56) Feng, X. Z.; Yang, Z.; Wang, L. J.; Bai, C. *Talanta* **1998**, *47*, 1223.
(57) Krishnamoorthy, P.; Sathyadevi, P.; Butorac, R. R.; Cowley, A. H.; Bhuvanesh, N. S. P.; Dharmaraj, N. *Dalton Trans.* **2012**, 4423.
(58) Sathyadevi, P.; Krishnamoorthy, P.; Jayanthi, E.; Butorac, R. R.; Cowley, A. H.; Dharmaraj, N. *Inorg. Chim. Acta* **2012**, *384*, 83.
(59) Ou, M. H.; Chen, Y. M.; Chang, Y. H.; Lu, W. K.; Liu, G. C.; Wang, Y. *Dalton Trans.* **2007**, 2749.
(60) Miller, J. N. *Proc. Anal. Div. Chem. Soc.* **1979**, *16*, 203.
(61) Tang, J. H.; Luan, F.; Chen, X. G. *Bioorg. Med. Chem.* **2006**, *149*, 3210.
(62) Gutteridge, J. M. C. *Chem.−Biol. Interact.* **1994**, *91*, 133.
(63) Khatua, S.; Choi, S. H.; Lee, J.; Huh, J. O.; Do, Y.; Churchill, D. G. *Inorg. Chem.* **2009**, *48*, 1799.
(64) Krishnamoorthy, P.; Sathyadevi, P.; Butorac, R. R.; Cowley, A. H.; Bhuvanesh, N. S. P.; Dharmaraj, N. *Dalton Trans.* **2012**, *41*, 4423.
(65) Khatua, S.; Choi, S. H.; Lee, J.; Kim, K.; Do, Y.; Churchill, D. G. *Inorg. Chem.* **2009**, *48*, 2993.